Final state control-based active compensation for backlash in vibration suppression of automobile powertrain

Masaki Hirata[a], Heisei Yonezawa[b], Ansei Yonezawa[c], and Itsuro Kajiwara[d*]

[a]*Division of Human Mechanical Systems and Design, Hokkaido University, N13, W8, Kita-ku, Sapporo 060-8628, Japan, E-mail:* tamasakishukatsu@gmail.com; [b]*Division of Mechanical and Aerospace Engineering, Hokkaido University, N13, W8, Kita-ku, Sapporo 060-8628, Japan, E-mail:* yonezawah@eng.hokudai.ac.jp; [c]*Division of Mechanical and Aerospace Engineering, Hokkaido University, N13, W8, Kita-ku, Sapporo 060-8628, Japan, E-mail:* ayonezawa@eng.hokudai.ac.jp; [d]*Division of Mechanical and Aerospace Engineering, Hokkaido University, N13, W8, Kita-ku, Sapporo 060-8628, Japan, E-mail:* ikajiwara@eng.hokudai.ac.jp

**Corresponding author*

Final state control-based active compensation for backlash in vibration suppression of automobile powertrain

Abstract

This paper proposes an effective backlash compensation method based on the final state control (FSC) for active vibration control of an automobile powertrain. Transient vibration of the powertrain caused by sudden changes in the engine torque significantly degrades the driving performance and driver comfort. In addition, the nonlinear characteristics owing to the backlash increase the adverse effects of these oscillations. To suppress the transient vibration of the powertrain, a controller is designed based on the mixed H_2/H_∞ control theory. Subsequently, to adjust for the vibration amplification owing to the backlash, we propose the application of a shock-reducing controller based on the FSC. Linearly decreasing the inertia weight in particle swarm optimization (LDWPSO) was applied to the design of this controller and parameters were optimized. Finally, simulations were conducted using the control method; the controller could prevent the occurrence of shocks owing to the gear collisions and achieved smooth acceleration.

Keywords : powertrain, drivetrain, anti-jerk control, backlash, final state control, nonlinear model

1. Introduction

An automobile powertrain is a power transmission system, which is responsible for transmitting the drive torque produced by the engine to the tyres. Vibration in the powertrain during a sudden change in drive torque deteriorates comfort and driving performance (Pan et al., 2022).

The differential gears in a powertrain have a gap between the gears (backlash), and sudden acceleration causes the gears to collide with each other, which generates shock torque and amplifies the amplitude of vibration. In addition, when the gears are not in contact, the engine cannot transfer the drive torque to the tyres, and the system structure of the powertrain changes. The nonlinear characteristics of system switching render the direct application of ordinary linear active controllers difficult (Vansevich, 2014; Vörös, 2009). Therefore, an active vibration control method is required for powertrains, which explicitly considers the effects of backlash.

Various active vibration control methods have been proposed for powertrains. In the research of Rodríguez et al. (2014), an electric vehicle equipped with an inboard motor was controlled by combining state feedback and tyre tracking loop to suppress the resonance. Vadamalu and Beidl (2016) proposed a model predictive controller for active vibration control of hybrid electric vehicles. Chen et al. (2022) combined model predictive control with the Butterworth filter control to suppress the torsional vibration in response to the sudden change in drive torque. An anti-jerk control based on the look-ahead model predictive controller is proposed, which improves the vibration suppression and tracking performance to the target value (Batra et al., 2019). However, in these studies, the backlash was not included and its effect was not considered.

Giancarlo and Mehdi (2006) proposed a state estimation method for backlash based on observable state quantities such as the torque from the engine and the angular velocity. Dhaouadi et al. (1994) considered the backlash issue and its effect on the control was estimated by applying the description function method; it was compensated by adding a first-order disturbance observer. Seldl et al. (1995) applied an artificial neural network to recognize the backlash and to study its smooth movement. Barbosa and Machado (2017) applied the descriptive function method with the discrete fractional order algorithm to the nonlinear control using PID control. Hunang et al. (2014) proposed a robust weighted gain-scheduling H_∞ control design. Wu et al. (2017) considered compensation of the blind band characteristics of nonlinear systems based on adaptive fuzzy control. Ponce et al. (2016) applied H_∞ control with motor position feedback to compensate the effect of the backlash. An attempt was made to suppress the vibration by applying the nonlinear problem owing to the backlash to the framework of the H_∞ control problem (Zuppa et al., 2013). In Lagerber and Egardt's research (2007), the backlash compensation function was improved by estimating the magnitude and state of the backlash using the Kalman filter.

However, the control systems in most of the previous studies are complicated; for example, they require the addition of viscous damping that does not exist in the gears. Therefore, a simpler and more versatile compensation method is required.

Several methods have been proposed for backlash compensation using model predictive control (MPC), such as control using horizon-1 MPC (Caruntu et al., 2016), MPC using four types of MPC controllers (Formentini et al., 2017), MPC with an additional element related to anti-shuffle control (Atabay et al., 2018), MPC combined with state estimation through observers (Rostalski et al., 2007), and MPC based on receding horizon sliding control (Li et al., 2017). Although MPC is a promising approach, the heavy computational burden of online optimization makes its implementation difficult. To compensate for the good control performance with a systematic approach, it is necessary to introduce model-based control. However, there have been few attempts to utilize the effective model-based control theory for both gear contact and non-contact situations.

One example of backlash compensation is the application of anti-jerk control. The Nissan LEAF was studied with a feed-forward controller to suppress torsional vibration (Kawamura et al., 2011). Truc et al. (2016) used a feed-forward controller based on flatness to follow a set trajectory. Yamaguchi et al. (2019) designed, a shock-reducing controller via final state control with an attempt to make the gears contact each other gently. Anti-jerk control is a model-based control; however, in these studies, modelling errors occurred between the real vehicle and anti-jerk control. It is necessary to consider such modelling errors by adding a proportional feedback controller to improve the performance.

Although a simple backlash compensation based on the mixed H_2/H_∞ control theory has already been proposed (Yonezawa et al., 2019), this has not been examined for the real vehicle model in detail.

The purpose of this study is to realize smooth acceleration of an automobile powertrain with nonlinear elements owing to the backlash by suppressing the vibration. To design a control system using the model-based approach, the automobile powertrain model including the nonlinear elements was modelled via a physical function model. A mixed H_2/H_∞ controller designed using the mixed H_2/H_∞ control theory was used to suppress the torsional vibration. The backlash was compensated by applying the final state control to reduce the collision shock by gently bringing the gears in contact with each other. The parameters used in the final state control were optimized by linearly decreasing the inertia weight in particle swarm optimization (LDWPSO) . A control system was constructed using these methods, and the effectiveness of the proposed method was verified by simulations.

This study offers the following contributions.

- The control system is light in real-time computation load and simple to implement. Specifically, the model-based control system is switched between the gear contact and non-contact.
- To suppress the torsional vibration during backlash coupling, a mixed H_2/H_∞ controller specialized in suppressing excessive control input and improving transient response is used.
- To compensate for the backlash, we propose the application of final state control (FSC). Unlike the trial-and-error compensation algorithms, the final state control method is a systematic design process and model-based control that makes effective use of the models. It is possible to design the system with explicit consideration of the output trajectory during the backlash disconnection.

- The optimization method can be used to design a controller that maximally reduces the shock caused through gear collision.
- The effectiveness of the proposed method was verified for a detailed realistic model.

2. Modelling of control object

2.1 Modelling of automobile powertrain using physical function model

The physical functional model (Hiramatsu et al., 2000; Sumida & Nagamatsu, 2001; Sumida et al., 2002; Yonezawa et al., 2019) represents each element of a mechanical system as a block diagram focusing on energy flow and deals with nonlinear elements by changing each characteristic moment by moment. If the parameters of the linear block diagram are calculated from theoretical equations and varied moment by moment, the nonlinear characteristics of the control target can be described. Figure 1 shows the configuration of an automobile powertrain.

Figure 2 shows the structure of the automobile powertrain represented by the physical function model. T_{eg} is the torque from the engine (engine torque) and the input to the automobile powertrain. The physical functional model consists of yellow mechanism model blocks and white linear blocks. The equations that represent the nonlinear elements are included in the mechanism model. The equations of the mechanism model are calculated according to the inputs, and the values of the nonlinear parameters are changed. The nonlinear parameters in this study are the clutch friction torque, parameters used in the gears contact judgement and running resistance. Table 1 shows the meanings and values of the parameters in Figure 2.

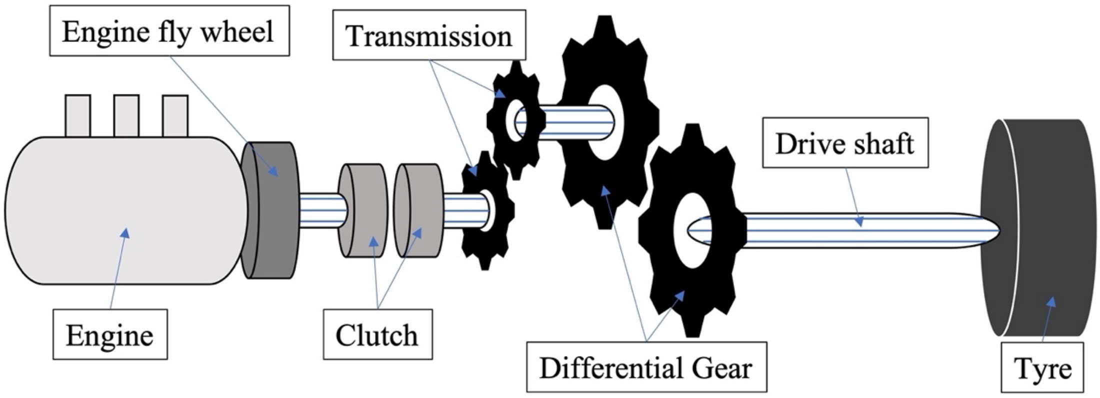

Figure 1. Schematic of automobile powertrain

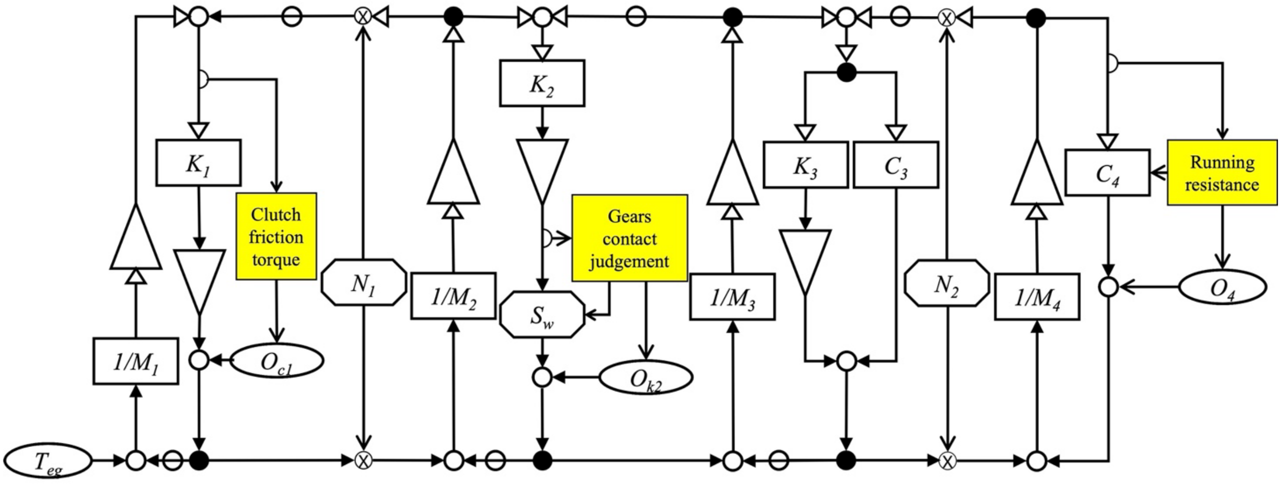

Figure 2. Physical function model of automobile powertrain

Table 1. Parameters in physical function model of automobile powertrain

Property	Symbol	Value	Unit
Equivalent inertia moment of engine, clutch, etc.	M_1	*2.3E-01*	kg m^2
Equivalent torsional rigidity of clutch and transmission	K_1	*1.1E-03*	N m^2
Gear ratio of transmission	N_1	*5.3E+00*	-
Inertia moment of input side of differential gear	M_2	*5.9E-02*	kg m^2
Torsional rigidity of differential gear	K_2	*5.7E+05*	N m^2
Inertia moment of output side of differential gear	M_3	*5.9E-02*	kg m^2
Torsional rigidity of drive shaft	K_3	*1.5E+04*	N m^2
Torsional damping of drive shaft	C_3	*7.7E+01*	kg m^2 s^{-1}
1/(radius of tyre)	N_2	*3.3E+00*	m^{-1}
Body mass	M_4	*1.5E+03*	kg
Engine torque	T_{eg}	-	Nm
Clutch friction torque	O_{c1}	-	Nm
Coefficient of gears contact judgement	S_w	-	-
Offset torque of gears contact judgement	O_{k2}	-	Nm
Slope of linearized running resistance	C_4	-	kg s^{-1}
Intercept of linearized running resistance	O_4	-	N

2.2 Equations and nonlinear parameters inside the mechanism model

2.2.1 Clutch friction torque

O_{c1} represents the clutch friction torque. The clutch friction torque is the torque generated by the frictional force owing to the difference in the rotational speed of the engine and tyre sides of the clutch. Assuming that the rotational speeds of the engine and tyre sides as ω_1 *and* ω_2, the value of O_{c1} is represented as:

$$\begin{aligned} O_{c1} &= 13.5\ Nm \qquad (\omega_1 - \omega_2 > 0) \\ O_{c1} &= -13.5\ Nm \qquad (\omega_1 - \omega_2 < 0) \\ O_{c1} &= 0\ Nm \qquad (\omega_1 - \omega_2 = 0) \end{aligned} \tag{1}$$

2.2.2. Gears contact judgement

S_w *and* O_{k2} were set as the parameters to identify the gear contact state during the backlash. S_w indicates whether the gears are in contact with each other, and O_{k2} is the offset torque to express the function of the dead zone effect in the backlash. Figure 3 demonstrates the relationship between the rotational angle difference $\Delta\theta$ between the input (engine-side) and output sides (tyre-side) of the differential gear and torsional torque T generated by the gear contact. The range of the backlash varies with the car; however, in this study, the range is assumed from *-2*° to *2*°. In this range, the gears are not in contact with each other, and torsional torque T is *0*. In contrast, when the rotational angle difference exceeds this range, the gears are in contact with each other and torsional torque T is generated. This relationship is expressed as:

$$T = S_w \cdot K_2 \cdot \Delta\theta' + O_{k2}$$

$$S_w = \begin{cases} 0, & |K_2 \cdot \Delta\theta'| < 20000 \\ 1, & K_2 \cdot \Delta\theta' \geq 20000 \\ 1, & K_2 \cdot \Delta\theta' \leq -20000 \end{cases} \tag{2}$$

$$O_{k2} = \begin{cases} 0, & |K_2 \cdot \Delta\theta'| < 20000 \\ -20000, & K_2 \cdot \Delta\theta' \geq 20000 \\ 20000, & K_2 \cdot \Delta\theta' \leq -20000 \end{cases}$$

where $\Delta\theta'$ is the conversion of $\Delta\theta$ into radians.

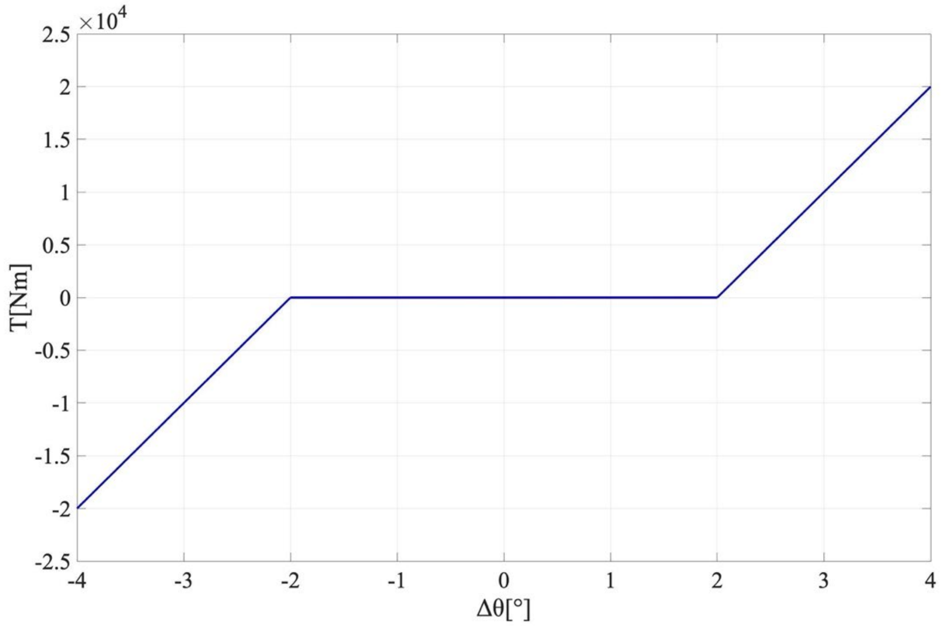

Figure 3. Relationship between $\Delta\theta$ and T

2.2.3 Running resistance

In this study, running resistance consists of air resistance F_a and rolling resistance F_r. Air resistance F_a is the force exerted by the air on the front surface of the vehicle body, and it can be expressed by Equation (3), using the vehicle speed v. The meanings and values of the parameters in Equation (3) are presented in Table 2.

$$F_a = \frac{1}{2} C_d \cdot \rho \cdot A_c \cdot v^2 \tag{3}$$

Rolling resistance F_r is the rotational resistance caused by the tyres and drive shafts. Experiments have shown that F_r is related to v. By approximating the relationship between F_r and v with the cubic equation for v, the following equation is obtained.

$$F_r = 0.0003v^3 + 0.0731v^2 - 2.2271v + 142.12 \tag{4}$$

The total of F_a and F_r is the running resistance F_b.

$$F_b = F_a + F_r \tag{5}$$

Using Equation (5), C_4 and O_4, from Table 1, are defined as:

$$C_4 = \frac{\mathrm{d}F_b}{\mathrm{d}v} \tag{6}$$

$$O_4 = F_b - C_4 \cdot v \tag{7}$$

Table 2. Parameters of air resistance formula

Property	Symbol	Value	Unit
Coefficient of drag	C_d	*0.3*	-
Air density (*20* °C, *1* atm)	ρ	*1.2*	kg m^{-3}
Frontal projected area	A_c	*2.2*	m^2

2.3 State and output equations of the automobile powertrain model

The state and output equations are derived for the automobile powertrain model obtained in Section 2.1. By defining the state quantities for each integrator shown in Figure 2, Equation (8) is obtained. The state quantity **x** and the input **u** are defined as in Equation (9). The properties of each state quantity in (9) are shown in Table 3. For the inputs, please refer Table 1 and 2. 2. In this study, the output y is the vehicle acceleration.

$$\begin{aligned} \dot{\mathbf{x}} &= \mathbf{Ax} + \mathbf{Bu} \\ y &= \mathbf{Cx} + \mathbf{Du} \end{aligned} \tag{8}$$

$$\mathbf{x} = \begin{bmatrix} x_{m1} \\ x_{k1} \\ x_{m2} \\ x_{k2} \\ x_{m3} \\ x_{k3} \\ x_{m4} \end{bmatrix}, \mathbf{u} = \begin{bmatrix} O_{c1} \\ O_{k2} \\ O_4 \\ T_{eg} \end{bmatrix} \tag{9}$$

Each coefficient matrix in Equation (8) is expressed as:

$$\mathbf{A} = \begin{bmatrix} 0 & -\frac{1}{M_1} & 0 & 0 & 0 & 0 & 0 \\ K_1 & 0 & -K_1 \cdot N_1 & 0 & 0 & 0 & 0 \\ 0 & \frac{N_1}{M_2} & 0 & -\frac{S_w}{M_2} & 0 & 0 & 0 \\ 0 & 0 & K_2 & 0 & -K_2 & 0 & 0 \\ 0 & 0 & 0 & \frac{S_w}{M_3} & -\frac{C_3}{M_3} & -\frac{1}{M_3} & C_3 \cdot \frac{N_2}{M_3} \\ 0 & 0 & 0 & 0 & K_3 & 0 & -K_3 \cdot N_2 \\ 0 & 0 & 0 & 0 & N_2 \cdot \frac{C_3}{M_4} & \frac{N_2}{M_4} & -\frac{C_3 \cdot {N_2}^2 + C_4}{M_4} \end{bmatrix}$$

$$\mathbf{B} = \begin{bmatrix} -\frac{1}{M_1} & 0 & 0 & \frac{1}{M_1} \\ 0 & 0 & 0 & 0 \\ \frac{N_1}{M_2} & -\frac{1}{M_2} & 0 & 0 \\ 0 & 0 & 0 & 0 \\ 0 & \frac{1}{M_3} & 0 & 0 \\ 0 & 0 & 0 & 0 \\ 0 & 0 & -\frac{1}{M_4} & 0 \end{bmatrix} \tag{10}$$

$$\mathbf{C} = \begin{bmatrix} 0 & 0 & 0 & 0 & \frac{N_2 \cdot C_3}{M_4} & \frac{N_2}{M_4} & -\frac{C_3 \cdot {N_2}^2 + C_4}{M_4} \end{bmatrix}$$

$$\mathbf{D} = \begin{bmatrix} 0 & 0 & -\frac{1}{M_4} & 0 \end{bmatrix}$$

Table 3. Parameters of state variable in automobile powertrain

Property	Symbol	Unit
Angular velocity of engine flywheel	x_{m1}	rad s^{-1}
Clutch spring torque	x_{k1}	Nm
Angular velocity on the input side of the differential gear	x_{m2}	rad s^{-1}
Relative angle of the input side of the differential gear to the output side	x_{k2}	rad
Angular velocity on the output side of the differential gear	x_{m3}	rad s^{-1}
Torsional torque of drive shaft	x_{k3}	Nm
Car velocity	x_{m4}	m s^{-1}

3. Controller design based on mixed H_2/H_∞ control theory

The mixed H_2/H_∞ control theory (Kaminer et al.,1993; Nishidome & Kajiwara, 2003; Wang et al., 2013; Yonezawa et al., 2019) is a control theory, in which the evaluated quantities to be controlled are expressed in terms of the H_2 and H_∞ norms. By evaluated in the H_2 and H_∞ norms, the transient response is improved and robust stability is ensured. In this study, the evaluated quantities are the vehicle acceleration and the engine torque T_{eg}. To improve the transient response, the vehicle acceleration is evaluated in the H_2 norm. To suppress the excessive T_{eg}, the T_{eg} is evaluated in the H_∞ norm.

In the mixed H_2/H_∞ control theory, effective vibration suppression and robustness are achieved using a weight function with large gain in the frequency band, for which the evaluation quantity is to be reduced. The target in this study is the first-order vibration mode (low-frequency vibration of approximately *7* Hz) of the acceleration. Therefore, the weight function applied to the acceleration is a Butterworth low-pass filter with cut-off frequency of *10* Hz. In contrast, if the T_{eg} is suppressed in the frequency band where the vibration is to be suppressed, the acceleration gain cannot be reduced effectively. In addition, the T_{eg} is the engine torque, and high frequency components cannot be output owing to the mechanism of the engine. Therefore, the weight function applied to the T_{eg} is a Butterworth high-pass filter with cut-off frequency of *50* Hz. The order of the low-pass and high-pass filters is set to *3*.

The mixed H_2/H_∞ control theory is designed for a generalized plant **G**, as shown in Figure 4, where W_2 is the low-pass filter and W_∞ is the high-pass filter. P is a linearised control target with nonlinear elements fixed. The generalized plant **G** is represented as:

$$\begin{bmatrix} \mathbf{z} \\ y_k \end{bmatrix} = \mathbf{G} \begin{bmatrix} \mathbf{w} \\ u_k \end{bmatrix} = \begin{bmatrix} \mathbf{G_{11}} & \mathbf{G_{12}} \\ \mathbf{G_{21}} & \mathbf{G_{22}} \end{bmatrix} \begin{bmatrix} \mathbf{w} \\ u_k \end{bmatrix}$$
$$\mathbf{z} = \begin{bmatrix} z_2 \\ z_\infty \end{bmatrix} \tag{11}$$

where $\mathbf{z}$ is the control quantity, y_k is the observed output, and u_k is the control input. $\mathbf{w}$ is the external input, which is the shock due to gear contact and brake. The variable z_2 is the controlled variable on the observed output (acceleration of the vehicle) after passing through the low-pass filter W_2 and z_∞ is the controlled variable on the control input (engine torque) after passing through the high-pass filter W_∞. Defining z_2 and z_∞ by this manner allows considering the trade-off between control performance and control input costs. The low-pass and high-pass filters are applied to z_2 and z_∞, respectively, to define the controlled frequency band appropriately.

If the controller is $\mathbf{K}_{\mathbf{H2H\infty}}$, the relation between u_k and y_k is expressed as:

$$u_k = \mathbf{K}_{\mathbf{H2H\infty}} y_k \tag{12}$$

Combining Equations (11) and (12), Equation (13) holds between the external input $\mathbf{w}$ and control quantities $\mathbf{z}$.

$$\begin{gathered} \mathbf{z} = \mathbf{G}_{\mathbf{zw}} \mathbf{w} \\ \mathbf{G}_{\mathbf{zw}} = \mathbf{G}_{\mathbf{11}} + \mathbf{G}_{\mathbf{12}} \mathbf{K}_{\mathbf{H2H\infty}} (1 - \mathbf{G}_{\mathbf{22}} \mathbf{K}_{\mathbf{H2H\infty}})^{-1} \mathbf{G}_{\mathbf{21}} \end{gathered} \tag{13}$$

In the mixed H_2/H_∞ control theory, the controller is designed to minimize the following equation:

$$\begin{gathered} \alpha \|\mathbf{G}_{\mathbf{z\infty w}}\|_\infty^2 + \beta \|\mathbf{G}_{\mathbf{z2w}}\|_2^2 \\ \alpha = 1.0, \beta = 1.0 \times 10^3 \end{gathered} \tag{14}$$

The variables α and β are the relative weights in evaluating the H_∞ *and* H_2 norms, respectively. In Equation (14), the performance indices for controlled response and control input costs are specified in H_2 norm and H_∞ norm, respectively. By adjusting α and β, designers can consider the trade-off between control performance and control input costs. In this study, the relative weights were determined by trial-and-error adjustments based on simulation tests to achieve both good transient response and control input cost savings. $\|\mathbf{G}_{z2w}\|_2$ is the H_2 norm of the transfer function $\mathbf{G}_{z2w}$ from $\mathbf{w}$ to z_2 and $\|\mathbf{G}_{z\infty w}\|_\infty$ is the H_∞ norm of the transfer function $\mathbf{G}_{z\infty w}$ from $\mathbf{w}$ to z_∞.

With only the control input designed using the methods, an offset appears between the acceleration response and target value. To improve the trackability to target value, a feed-forward input is added.

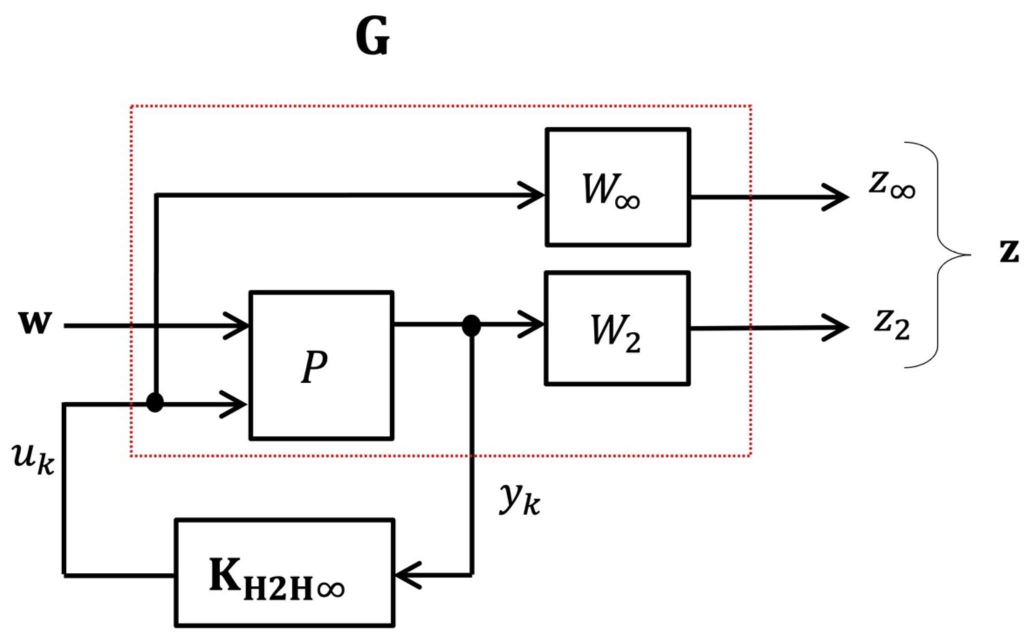

Figure 4. Block diagram of generalized plant **G**

4. Backlash compensation using final state control

4.1 About final state control

When the pair gears are not in contact with each other, the automobile powertrain cannot transmit the engine torque to the tyre-side and the change in vehicle acceleration is insignificant regardless of the engine torque. The longer the non-contact time (dead time), the longer is the time lag between the driver-directed acceleration timing and vehicle's acceleration. This time lag causes discomfort to the driver. While the gears are not in contact, the mixed H_2/H_∞ controller tries to follow the target value, so the control input is gradually increased. The longer the time lag, the more excessive the control input becomes when the gears make contact and bigger the shock when the gears make contact. Therefore, the gears should make contact as soon as possible so that the shocks at the time of contact are suppressed. By systematically designing these two requirements, the trial-and-error process to compensate for backlash can be eliminated and burden on the designer can be reduced. In addition, off-line design of control inputs to realize loose gear contact can reduce the computational load during simulation and implementation. In this study, we propose the application of final state control (FSC) (Hirata et al., 2005; Totani & Nishimura, 1994) as a compensation for backlash.

Final state control is a control method for controllable one-input discrete-time systems; it is expressed in Equation (15), in which the control input is obtained from the initial state $\mathbf{x_F}$ (0) to final state $\mathbf{x_F}$ (N_{FSC}) *in* N_{FSC} steps.

$$\mathbf{x_F}\ (k+1) = \mathbf{A_F}\mathbf{x_F}\ (k) + \mathbf{B_F}u_F\ (k) \tag{15}$$

Where, m is a positive integer, $\mathbf{A_F}$ is a real matrix of $m \times m$ size, and $\mathbf{B_F}$ is a real matrix of $m \times 1$ size. Such an input is not uniquely definite in general. Therefore, for any positive definite matrix $\mathbf{Q_F}$,

$$J = \mathbf{U}_{\mathbf{FSC}}^{\mathrm{T}}\mathbf{Q_F}\mathbf{U_{FSC}}. \tag{16}$$

The control input that minimizes Equation (16) is obtained; however, let $\mathbf{U_{FSC}}$ be defined as:

$$\mathbf{U_{FSC}} := (u_F\ (0),\quad u_F\ (1),\quad \dots\quad u_F\ (N_{FSC}-1))^T \tag{17}$$

Hirata et al. (2005) show that the following theorem is obtained by defining $\mathbf{\Sigma}$ as Equation (18).

$$\mathbf{\Sigma} = [\mathbf{A_F}^{N_{FSC}-1}\mathbf{B_F},\quad \mathbf{A_F}^{N_{FSC}-2}\mathbf{B_F},\quad \dots\quad \mathbf{B_F}] \tag{18}$$

(Theorem) In Equation (15), the input $u_F\ (k)$ that minimizes Equation (16) among the inputs $u_F\ (k)$ to reach the final state $\mathbf{x_F}\ (N_{FSC})$ from the initial state $\mathbf{x_F}\ (0)$ is expressed as:

$$\begin{aligned}\mathbf{U_{FSC}} = \mathbf{Q_F}^{-1}\mathbf{\Sigma}^T(\mathbf{\Sigma}\mathbf{Q_F}^{-1}\mathbf{\Sigma}^T)^{-1}\{&\mathbf{x_F}\ (N_{FSC}) \\ &- \mathbf{A_F}^{N_{FSC}}\mathbf{x_F}\ (0)\} \\ N_{FSC} \geq m\end{aligned} \tag{19}$$

(Hirata et al., 2005, p525)
For more details on final state control, please refer the research of Hirata et al. (2005) and the research of Totani & Nishimura (1994).

4.2 Application of final state control to automobile powertrain model

Based on Equation (19), we consider an application of the backlash problem of automobile powertrain. If **A** *and* **B** in Equation (10) are used as $\mathbf{A_F}$ *and* $\mathbf{B_F}$ in Equation (15), the number of state quantities becomes seven. It increases the designer's burden. Therefore, one-input discrete-time system is set up separately, in which only the element related to the differential gear is used as the state quantity $\mathbf{x_F}$. As introduced in Section 2.2.2, the difference in rotation angles between the engine-side and tyre-side of the differential gears is in the range from *-2*° to *2*°. Meanwhile, the relative angles of the engine-side viewed from the tyre-side are in the range from *0*° to *4*°. Further, when considering the behaviour of the engine-side viewed from the tyre-side, the tyre-side can be considered relatively stationary. Therefore, $\mathbf{x_F}$ is set as the relative angle and relative angular velocity of the engine-side inertia as viewed from the tyre-side inertia inside the differential gears. Via this setting of $\mathbf{x_F}$, the tyre-side inertia can be omitted from the system design.

From the automobile powertrain model shown in Figure 2, a discrete-time system was constructed with the relative angle and relative angular velocity as state quantities. Figure 5 shows the part of the control target used in the final state control. As $\mathbf{x_F}$ is a relative value from the tyre-side, the downstream systems after the tyre-side are not considered.

First, from the engine-side inertia in Figure 5, the equivalent torsional rigidity of clutch and transmission K_1 and the clutch friction torque O_{c1} are omitted from the model. This is because these elements are relatively small in the engine-side inertia and are not considered to have a significant influence on the reproduction of the powertrain behaviour.

If K_1 and O_{c1} are omitted, the engine-side inertia becomes as illustrated in Figure 6. If the force generated inside the transmission is F, the equations of motion for the rotating system of the crankshaft and engine-side differential gear are Equation (20) and Equation (21), respectively. The value of t is time. T_{eg} is the engine torque. M_1 is the equivalent inertia moment of engine, clutch, etc. M_2 is the inertia moment of input side (engine-side) of differential gear. r_1 and r_2 are the gear radii on the engine and tyre-sides of the transmission, respectively. θ_1 and θ_2 are the angles on the engine and tyre-side of the transmission, respectively. Because the transmission of tyre-side and differential gear are connected, θ_2 is also the relative angle of the engine-side gear of the differential gear viewed from the tyre-side gear.

$$M_1 \cdot \ddot{\theta}_1 (t) = T_{eg} - F \cdot r_1 \tag{20}$$

$$M_2 \cdot \ddot{\theta}_2\,(t) = F \cdot r_2 \tag{21}$$

As the gears of the transmission are in contact with each other, Equation (22) holds.

$$r_1 \cdot \ddot{\theta}_1\,(t) = r_2 \cdot \ddot{\theta}_2\,(t) \tag{22}$$

Combining Equations (20)-(22), we obtain Equation (23), where N_1 is the gear ratio of the transmission.

$$\begin{aligned} &\left(N_1 \cdot M_1 + \frac{M_2}{N_1}\right)\ddot{\theta}_2\,(t) = T_{eg} \\ &N_1 = \frac{r_1}{r_2} \end{aligned} \tag{23}$$

The system to be controlled used in final state control is set as in Equation (24).

$$\begin{bmatrix} \dot{\theta}_2\,(t) \\ \ddot{\theta}_2\,(t) \end{bmatrix} = \begin{bmatrix} 0 & 1 \\ 0 & 0 \end{bmatrix} \begin{bmatrix} \theta_2\,(t) \\ \dot{\theta}_2\,(t) \end{bmatrix} + \begin{bmatrix} 0 \\ \dfrac{1}{N_1 \cdot M_1 + \dfrac{M_2}{\mathrm{N}_1}} \end{bmatrix} T_{eg} \tag{24}$$

Comparing Equation (24) with Equation (15), we get $\mathbf{A_F}$ and $\mathbf{B_F}$ as Equation (25). Discretizing Equation (25), the obtained coefficient matrix is used in the final state control.

$$\mathbf{A_F} = \begin{bmatrix} 0 & 1 \\ 0 & 0 \end{bmatrix}$$

$$\mathbf{B_F} = \begin{bmatrix} 0 \\ \dfrac{1}{N_1 \cdot M_1 + \dfrac{M_2}{N_1}} \end{bmatrix} \tag{25}$$

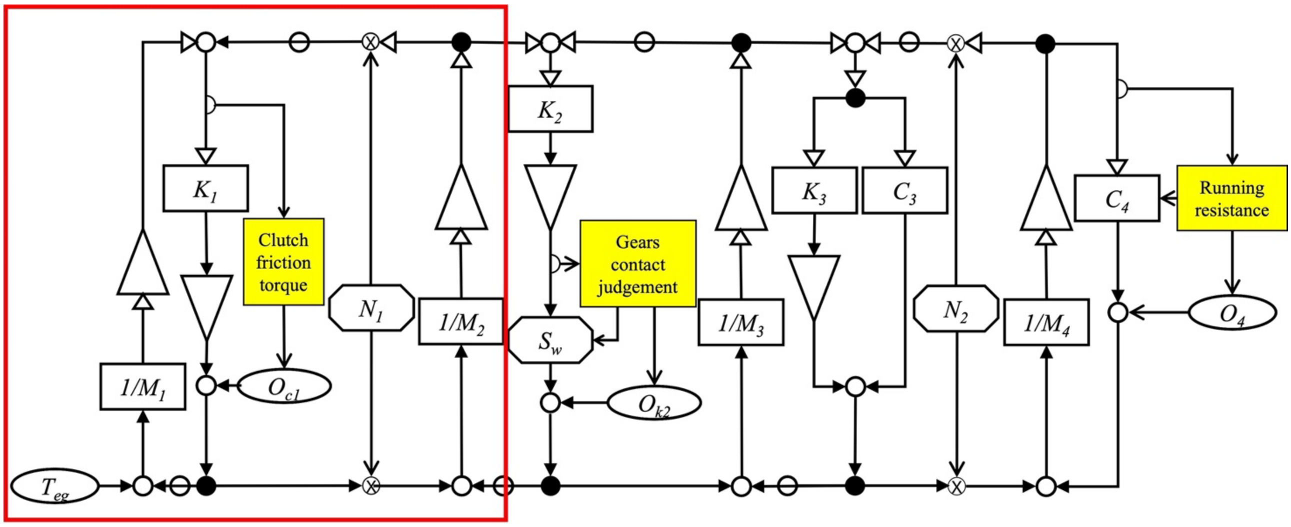

Figure 5. Control target used in final state control

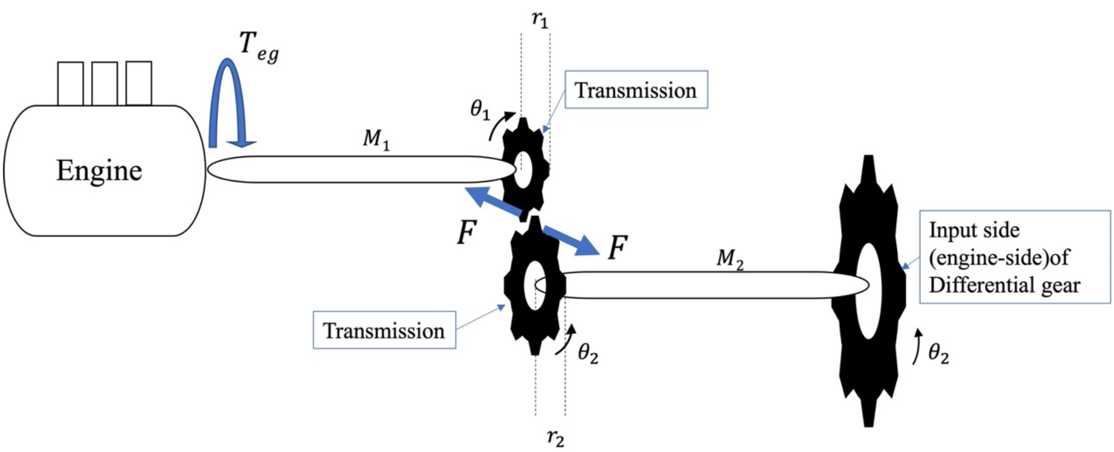

Figure 6. Simplification of engine-side inertia

4.3 Final state control optimization using LDWPSO

When driving a car, there is dead time between the time when the driver presses the accelerator pedal and time when the car accelerates. This is because the driver may feel fear if the car behaves too well to the accelerator pedal operation. In this study, final state control is used during the dead time to reduce the gear collision shock caused to the backlash.

The initial state, the final state and the dead time should be determined by the designer. One way to determine these values is by trial-and-error adjustment. However, this increases the designer's burden. Therefore, these values are adjusted by linearly decreasing the inertia weight in particle swarm optimization (LDWPSO) (Shi & Eberhart, 1998, 1999) to search for the parameters, which maximally suppress the vibration.

The particle swarm optimization (PSO) method is a heuristic optimization method inspired by the social flocking behaviour of birds, which share their experiences. (Marini & Walczak, 2015; Zietkiewicz et al., 2020) LDWPSO is an improved version of PSO and a method that linearly decreases the weight of velocity inertia at each iteration. At the beginning of the search, the weights are large to enable wide search; as the number of iterations progresses, the weights become smaller. By decreasing the weights, the particles are more likely to converge to a single point, which improves the convergence to the true optimal solution.

The flow of LDWPSO is described as follows. First, the designer sets the number of particles. In this study, the number of particles was set to *100*. The swarm is initialized by randomly assigning an initial velocity and position to each particle. As each particle moves, it evaluates its current position with respect to the objective function to be minimized. The objective function F_{Ob} to be minimized by LDWPSO is shown in Equation (26). The meanings and values of the parameters of the objective function are presented in Table 4.

$$F_{Ob} = W_e \cdot \|A_T - A_B\|_2 + W_u \cdot \|T_{eg}\|_2 \tag{26}$$

In the vibration control of an automobile powertrain, the acceleration response is required to follow the target value, while the engine torque (control input) is required not to be excessive. Therefore, considering the two norms of the difference between the target value and vehicle acceleration, and the engine torque, we have developed an objective function that can consider both the following to the target value and the engine torque. Because the oscillations occur approximately *2.0* s after the start of the simulation, the period for evaluation was set as from *1.5* to *2.3* s (refer the simulation results in Chapter 5).

The parameters that minimize Equation (26) are searched for as each particle updates its velocity and position. Each particle searches for the parameter that minimizes the evaluation function by updating the following two equations.

$$\begin{aligned} v_{id}\,(t+1) = w\,(t) v_{id}\,(t) \\ + c_1 R_1 \big(p_{id}\,(t) - x_{id}\,(t)\big) \\ + c_2 R_2 \left(p_{gd}\,(t) - x_{id}\,(t)\right) \end{aligned} \tag{27}$$

$$x_{id}\,(t+1) = x_{id}\,(t) + v_{id}\,(t+1) \tag{28}$$

Equations (27) and (28) are called the velocity and position update equations, respectively. The meanings and values of each parameter in the equations are listed in Table 5. For each particle, if the fitness value at the current position $x_{id}\,(t)$ is smaller than the current best position $p_{id}\,(t)$, the particle updates its own best position p_{id} (t). The p_{id} (t) of each particle is compared, and if any of them has the smallest fitness value of the group until that time, its position is updated as p_{gd} (t). In Equation (27), w (t) is expressed as:

$$w\ (t) = W_{max} - \frac{W_{max} - W_{min}}{t_{max}} \cdot t \tag{29}$$

Where, W_{max} and W_{min} represent the initial and final weights respectively. t_{max} is the maximum number of iterations, which in this study is *100*. From Equation (29), w (t) decreases linearly from W_{max} to W_{min} with each increase in the number of iterations. This reduces the influence of v_{id} (t) in Equation (27) and increases the influence of terms related to p_{id} (t) and p_{gd} (t) relatively more. Using large initial weights in the early stage of the search and small final weights in the end of the search, particles approach p_{id} (t) and p_{gd} (t) more readily and converge to a single point more easily than in the conventional PSO. In this study, W_{max} and W_{min} are set to *0.9* and *0.4*, respectively.

The three design variables adjusted by LDWPSO are the dead time T_{FSC}, relative angle $\theta_2\ (N_{FSC})$, and relative angular velocity $\dot{\theta}_2\ (N_{FSC})$ in the final state. In most cases, the present car dead time is assumed approximately *0.05* s. As the range of backlash is in the range from *-2*° to *2*°, the relative angle in the final state should be *4*°. In addition, the relative angular velocity in the final state should be *0* rad s^{-1} to contact the gear as gently as possible. However, excessive control input is required to reach closer to these values. Therefore, it is necessary to determine parameters that minimize the dead time and simultaneously avoid excessive control input to bring the gears in contact. Table 6 lists the parameters before optimization. N_{FSC} is obtained by dividing T_{FSC} by T_s.

Table 7 presents the results of optimization using LDWPSO. The adjusted results show that T_{FSC} is slightly longer than *0.05* s; however, short enough to bring the gears in contact. The relative angular velocity $\dot{\theta}_2\ (N_{FSC})$ was adjusted at *0* rad s^{-1}; however, the relative angle $\theta_2\ (N_{FSC})$ was adjusted at an angle smaller than *4*° owing to the effect of running resistance. When the engine gear moves closer to the tyre gear, the tyre gear also moves relatively closer to the engine gear. Therefore, the angle, at which the engine gear must move for the gears to make contact is smaller than *4*°.

In addition, basic PSO and LDWPSO were compared. In the basic PSO, the optimization is performed by setting *w* (*t*) in Equation (29) to *1*. The values of the objective function F_{Ob} in Equation (26) before optimization, after optimization via basic PSO, and after optimization via LDWPSO are listed in Table 8. The fact that LDWPSO has a smaller value of the objective function than that of the basic PSO indicates that LDWPSO has an advantage over the basic PSO.

Using the optimization parameters, the behaviour of the control input in Equation (19) is shown in Figure 7. In Figure 7, $\mathbf{U}_{FSC}$ is the positive torque at the beginning, and then $\mathbf{U}_{FSC}$ gradually decreases. Immediately after the rattling starts, positive torque closes the backlash forcefully. When the gears make contact, negative torque reduces the momentum, so that the contact is gradual without generating a shock.

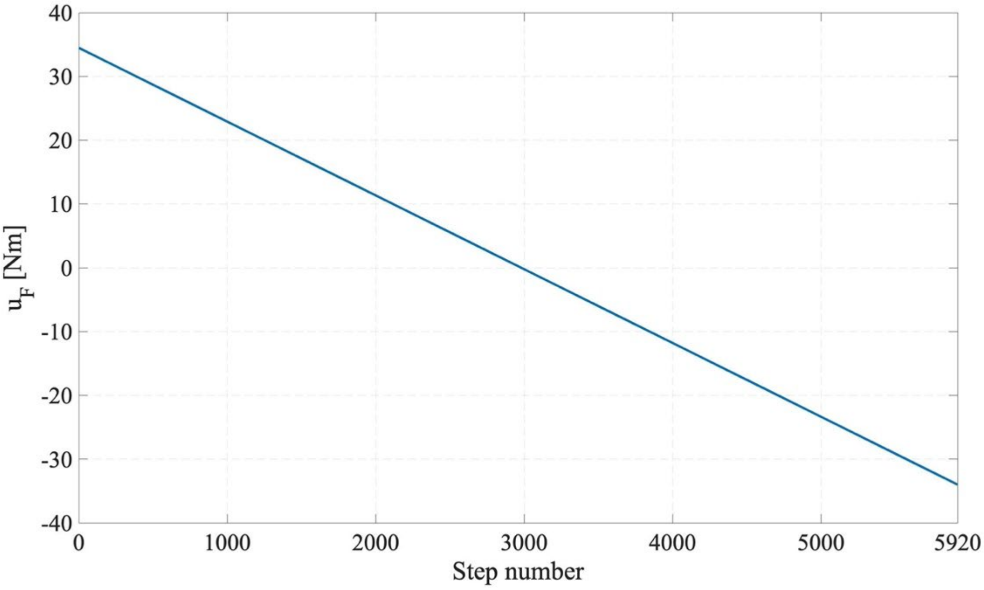

Figure 7. Control input of final state control

Table 4. Parameters of LDWPSO's objective function

Property	Symbol	Value	Unit
Inertia weight of acceleration norm	W_e	*1*	-
Inertia weight of engine torque norm	W_u	*0.01*	-
Target acceleration (*1.5~2.3* s)	A_B	-	m s^{-2}
Vehicle acceleration (*1.5~2.3* s)	A_T	-	m s^{-2}
Engine torque (*1.5~2.3* s)	T_{eg}	-	Nm
2-norm of ·	$\|\cdot\|_2$	-	-

Table 5. Parameters of velocity update formula and position update formula

Property	Symbol	Value
Particle number	i	*1–100*
Iteration number	t	*1–100*
Dimension number	d	*1–3*
Cognitive learning rate	C_1	*0.9*
Social learning rate	C_2	*0.9*
Random number in the range [*0.0*, *1.0*]	R_1	[*0.0*, *1.0*]
Random number in the range [*0.0*, *1.0*]	R_2	[*0.0*, *1.0*]
Inertia weight on velocity	w	-
Rate of change in position (velocity) of the i-th particle in the d-th dimension	v_{id}	-
Position of the i-th particle in the d-th dimension	x_{id}	-
Personal best position of the i-th particle in the d-th dimension	p_{id}	-
Global best position in the d-th dimension	p_{gd}	-

Table 6. Parameters of FSC before optimization by LDWPSO

Property	Symbol	Value	Unit
Time of FSC	T_{FSC}	*0.05*	s
Sampling time	T_s	*0.00002*	s
Step number of FSC	N_{FSC}	*2500*	-
Initial state of θ_2	$\theta_2\ (0)$	*0*	°
Initial state of $\dot{\theta}_2$	$\dot{\theta}_2\ (0)$	*0*	rad s^{-1}
Initial state of θ_2	$\theta_2\ (N_{FSC})$	*4*	°
Initial state of $\dot{\theta}_2$	$\dot{\theta}_2\ (N_{FSC})$	*0*	rad s^{-1}

Table 7. Parameters of FSC after optimization by LDWPSO

Property	Symbol	Value	Unit
Time of FSC	T_{FSC}	*0.1192*	s
Sampling time	T_s	*0.00002*	s
Step number of FSC	N_{FSC}	*5960*	-
Initial state of θ_2	$\theta_2\ (0)$	*0*	°
Initial state of $\dot{\theta}_2$	$\dot{\theta}_2\ (0)$	*0*	rad s^{-1}
Initial state of θ_2	$\theta_2\ (N_{FSC})$	*3.7302*	°
Initial state of $\dot{\theta}_2$	$\dot{\theta}_2\ (N_{FSC})$	*0*	rad s^{-1}

Table 8. Objective function values of each PSO

	Before optimization	Basic PSO	LDWPSO
The value of objective function	*31.9083*	*3.8139*	*3.8111*

4.4 Control system configuration

The control system was configured using the control methods introduced in the previous sections. The configuration of the control system is shown in Figure 8. $\mathbf{K}_{\mathbf{H2H\infty}}$ is the mixed H_2/H_∞ controller, *P* is the automobile powertrain model, $\mathbf{U}_{\mathbf{FSC}}$ is the controller for final state control, and *FF input* is the feed-forward input. To make the vehicle acceleration follow the target value, the difference between the target value *r* and vehicle acceleration *y* is input to the mixed H_2/H_∞ controller.

To accommodate the system characteristic fluctuations in the automobile powertrain model due to the backlash and to suppress the amplification of vibration caused by the gear contact, the control input of $\mathbf{U}_{\mathbf{FSC}}$ is input to the automobile powertrain. However, $\mathbf{U}_{\mathbf{FSC}}$ cannot compensate for the suppression of torsional vibration and trackability to the target value *r*. Contrarily, the mixed H_2/H_∞ controller and feed-forward input can compensate for the characteristics not considered in the final state control; however, they cannot compensate for the shock due to backlash.

Therefore, the engine torque input to the automobile powertrain is switched for control.

The switching of engine torque is described as follows. From the beginning of the simulation until the driver starts pressing the accelerator pedal, the engine torque is assumed the sum of the input from the mixed H_2/H_∞ controller and feed-forward input. The control input for the final state control is the engine torque between when the driver starts pressing the accelerator pedal and when the acceleration starts. When the gears meet each other through the control input of final state control, the vehicle starts to accelerate. At this point, the engine torque is again returned to the sum of the input from the mixed H_2/H_∞ controller and feed-forward input to suppress the torsional vibration. Figure 9 presents an illustration of the switching of the control inputs to control target. In this figure, the period from the start of simulation to when the driver starts pressing the accelerator pedal and the period after the gear comes in contact correspond to the contact mode. The period from when the driver starts pressing the accelerator pedal to when the acceleration starts corresponds to the backlash mode.

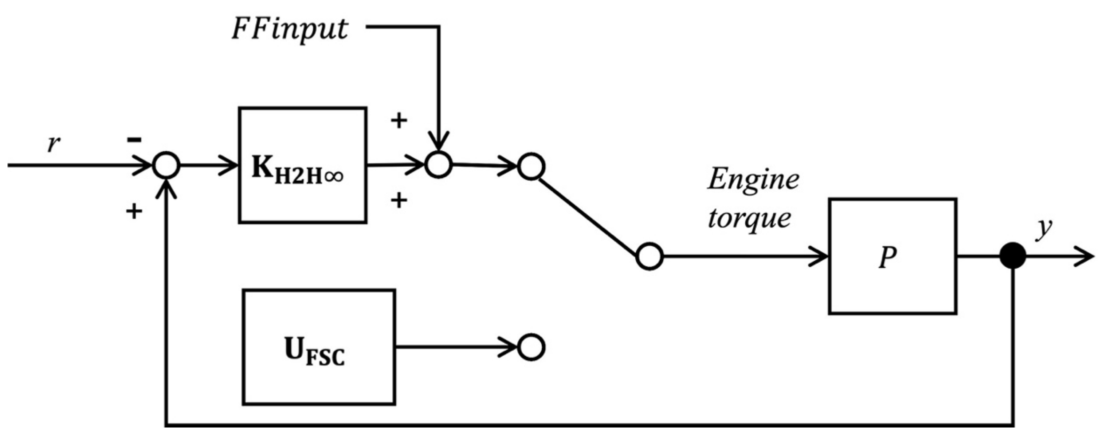

Figure 8. Block diagram of control system

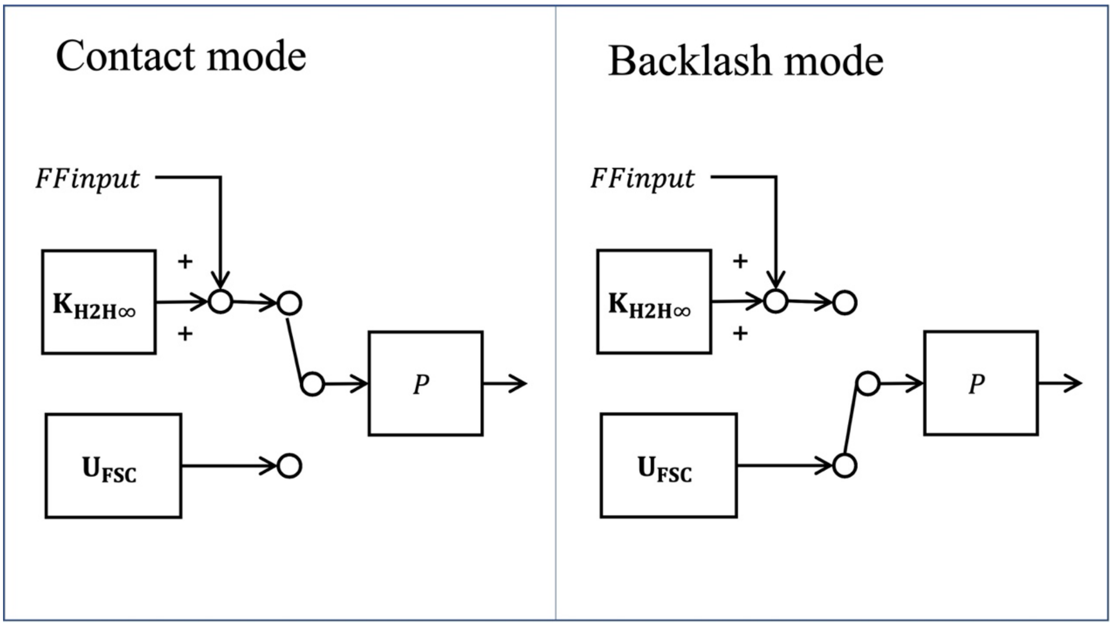

Figure 9. Switching controllers

5. Verification of simulation

5.1 Simulation conditions

In this study, the simulation was performed under the condition that the car was first in a state of gradual deceleration, and then in a state of rapid acceleration. This means that the driver released the accelerator pedal and then accelerated by pressing the accelerator pedal. The rapid acceleration produced a low-frequency vibration. Because the low-frequency vibration interferes with the driving performance and riding comfort of the automobiles, the resonance to be suppressed is the low-frequency vibration of the first-order natural frequency (*7* Hz) of the automobile powertrain. The simulation time was *3.5* s, and engine torque switched *2.0* s after the start of the simulation. The sampling period was set to *50* kHz. The initial conditions of the state quantities set for the automobile powertrain are listed in Table 9, to reproduce the behaviour of the automobile in the deceleration state.

Table 9. Parameters of initial state value in automobile powertrain

Property	Symbol	Unit
Angular velocity of engine flywheel	$1416.16084 \cdot 2\pi/60$	rad s^{-1}
Clutch spring torque	$-3.418/K_1$	Nm
Angular velocity on the input side of the differential gear	$1416.16084 \cdot 2\pi/(60 \cdot N_1)$	rad s^{-1}
Relative angle of the input side of the differential gear to the output side	$-2 \cdot \pi/180$	rad
Angular velocity on the output side of the differential gear	$1416.16084 \cdot 2\pi/(60 \cdot N_1)$	rad s^{-1}
Torsional torque of drive shaft	$-18.18/K_3$	Nm
Car velocity	$1416.16084 \cdot 2\pi/(60 \cdot N_1 \cdot N_2)$	m s^{-1}

5.2 Simulation results

Figure 10 shows the simulation results of the vibration control of an automobile powertrain when the engine torque is changed from *-4* Nm to *16* Nm. The upper graph shows the time response of the vehicle acceleration and lower graph shows the time response of the engine torque (control input). The red lines show the results obtained using the proposed method with the mixed H_2/H_∞ control and final state control. The blue lines show the results of open-loop response. The green line shows the ideal acceleration response (target acceleration) that should be realized by the control.

The blue line shows that the acceleration response is delayed in relation to the rise in the target value, and that overshooting occurs. This indicates that the backlash is causing the automobile powertrain to act as a dead zone, and that the gears are contacting each other, resulting in a shock. After the overshooting occurs, a small negative constant acceleration is observed for some time, and then overshooting occurs again. The constant acceleration indicates that the shock of contact causes the gears to separate once again. After that, the gears contact each other again and the momentum of the contact causes another shock; this behaviour is repeated about twice. Figure 11 shows the behaviour of the relative angles in the differential gears. It can be seen from the movement of the blue lines in Figures 10 and Figure 11 that the gears are separated when the acceleration reaches a certain value.

The acceleration response of the red line in Figure 10 shows that the vehicle begins to accelerate in accordance with the rise in the target value by applying the mixed H_2/H_∞ controller and final state control, and that a good transient response is realized by suppressing the vibration. Furthermore, Figure 11 shows that the gears gradually move from deceleration to the acceleration during the waste time and that they gently contact each other approximately *2.0* s before the acceleration starts. The gentle contact of the gears suppresses the increase in vibration amplitude caused by the collision, resulting in smooth acceleration.

To verify the effectiveness of final state control, Figure 12 compares the results with and without the final state control. The red line shows the result with final state control, and black line shows the result without final state control; the control is always performed by the mixed H_2/H_∞ controller. Specifically, the black line corresponds to the case in Figure 9 where the control is always performed in the contact mode. When the final state control is not applied, the acceleration timing is delayed and an overshooting occurs in the acceleration response. This indicates that the control by the mixed H_2/H_∞ controller alone cannot avoid the occurrence of shocks owing to the backlash collision and cannot suppress the overshooting. The mixed H_2/H_∞ controller cannot cope with the backlash problems. Applying the final state control, the control system can cope with the backlash problems.

To demonstrate the effectiveness of the parameter tuning of the final state control by LDWPSO, the responses before and after the optimization are compared. Figure 13 compares the responses before and after parameter adjustment. The black line shows the results before parameter adjustment, and red line shows the results after parameter adjustment. Refer Table 6 for the parameters of final state control in the black line and Table 7 for the parameters in the red line. Comparing with the black line and red line of the acceleration responses, the red line shows that the acceleration timing is faster and impact caused by the gear contact is suppressed. In addition, it is necessary for the suppression of vibrations to be cost-effective as reducing fuel consumption and saving energy are crucial. The engine torque behaviour of the black line is approximately *200* Nm immediately after shifting to the backlash mode. On the other hand, the output is approximately *30* Nm after the parameter adjustment. This indicates that vibration control can be achieved with less control input by adjusting the parameters using LDWPSO. The fact that the vibration can be sufficiently suppressed even though the control input is smaller than that before the adjustment indicates the effectiveness of the parameter optimization via LDWPSO.

To demonstrate that the proposed method can realize good control performance under other acceleration conditions, the simulation result with another maneuver when the engine torque is changed from *-4* Nm to *180* Nm is shown in Figure 14. The acceleration response indicated by the red line in Figure 14 shows that the proposed control system provides the good tracking performance to the target acceleration and sufficiently reduces the vibrations. This result indicates that the controller can maintain the control performance even when the acceleration conditions change.

These results indicate that the proposed method is effective in suppressing the overshooting caused by the backlash.

It is necessary to consider the aspects related to model uncertainty in the controller design process to deal with a real scenario of the application to automobile powertrain. To deal with model uncertainty, some approaches such as the application of a controller that adjusts the gain online (Jung & Glover, 2005; Gagliardi et al., 2022), the approach to guarantee the robustness of the control system by considering a conditional expression for closed-loop system (Chamaillard et al., 2004) and the application of final state control that takes into account feedback factors can be examined. It will be considered to combine these approaches and the proposed method in the future.

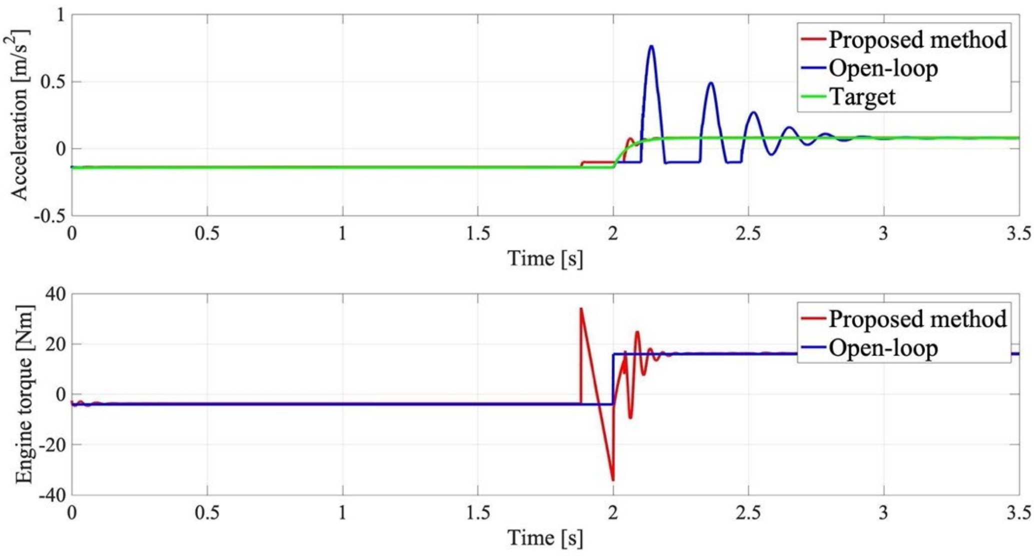

Figure 10. Simulation result (from *-4* Nm to *16* Nm)

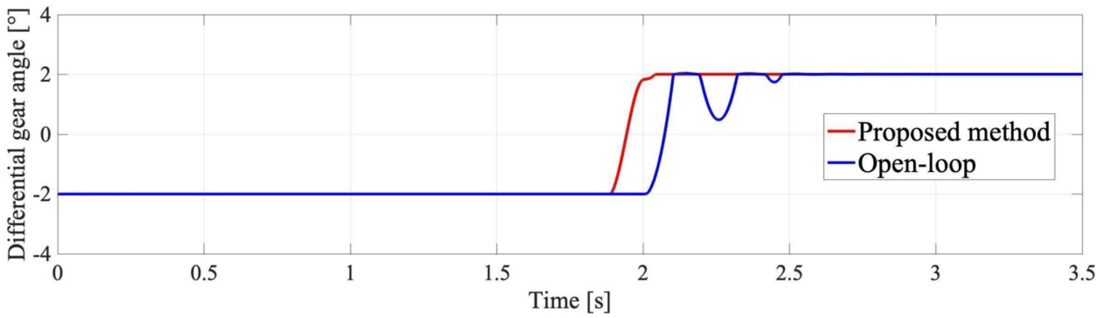

Figure 11. Behaviour of angle in differential gear

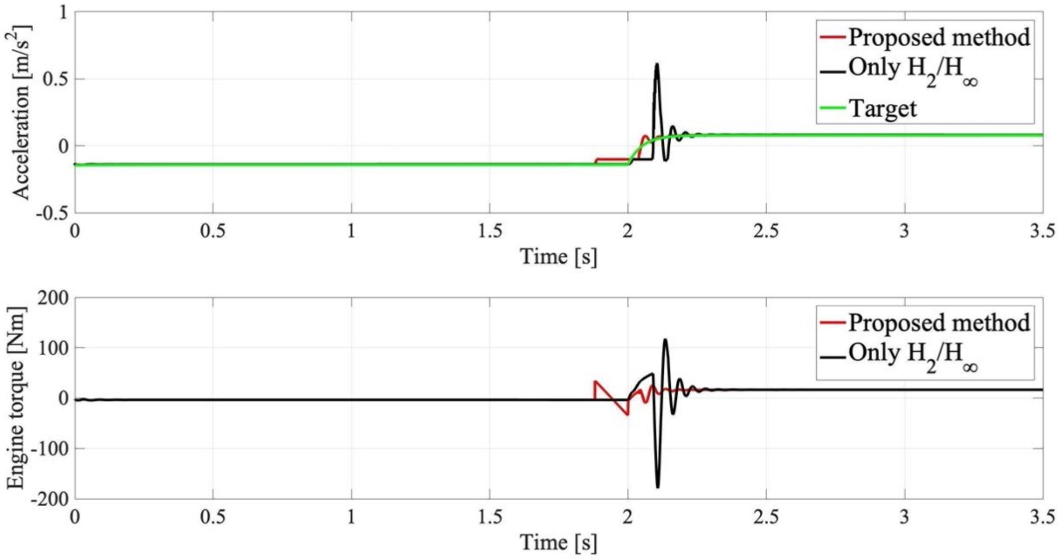

Figure 12. Comparison of responses between proposed control strategy and only H_2/H_∞ control

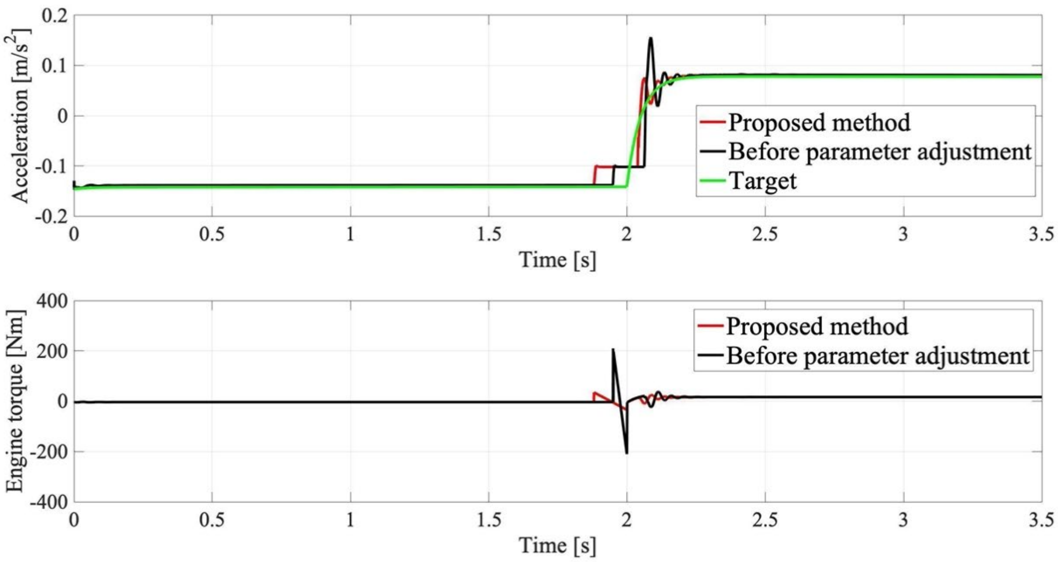

Figure 13. Comparison of responses between proposed control strategy and before parameters optimization

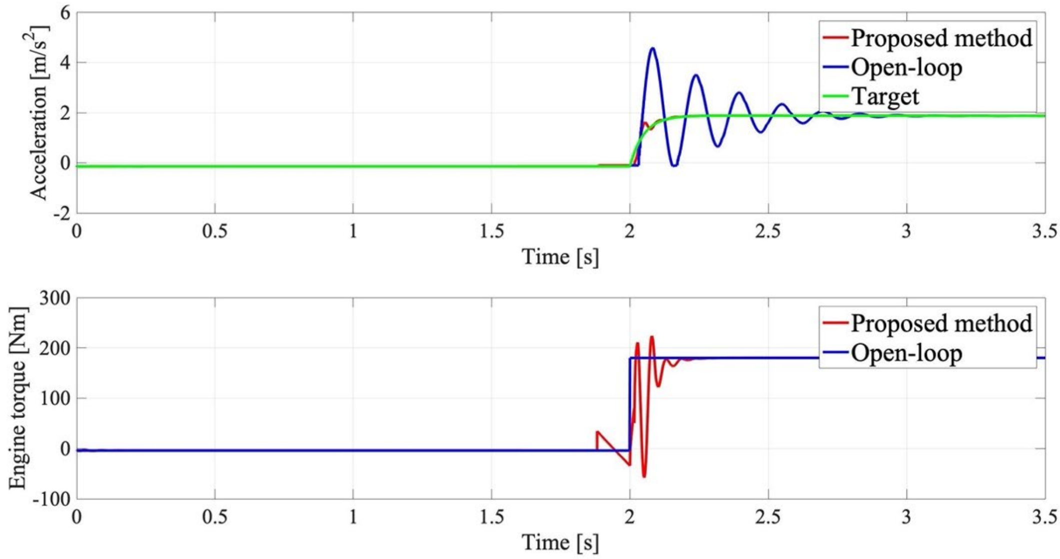

Figure 14. Simulation result (from *-4* Nm to *180* Nm)

6. Conclusion

In this study, an active vibration control method is proposed for an automobile powertrain with nonlinear elements related to the backlash by applying the final state control. A physical function model was used to model the characteristics of the automobile powertrain. Next, a mixed H_2/H_∞ controller was designed based on the mixed H_2/H_∞ control theory. Application of the final state control to compensate for the backlash problem was proposed in this study. LDWPSO was applied to the parameters to be set by the designer in the final state control, and effective parameters for vibration control were explored. Finally, simulation verification of these control methods was conducted. Based on the simulation results, the shock caused by gear collision could be suppressed by gently bringing the gears in contact with each other. The parameter optimization using LDWPSO improved the tracking performance to the target value. Also, backlash compensation was achieved with less energy consumption for vibration control.

Future studies will include ensuring robustness against parameter perturbations in the powertrain. As the controller based on the final state control is a feed-forward controller, it may not be able to cope with the parameter perturbations.

In addition, the engine has difficulty in outputting negative torque in the wide range at various speeds accurately. One effective solution to this issue is to apply the proposed control system to a powertrain mechanism in hybrid electric vehicles (HEVs) and electric vehicles (EVs), which are much more capable on torque response and negative torque. Therefore, it will be necessary to study the implementation of this method in HEVs and EVs in the future.

Disclosure statement

The authors report no conflict of interest.

References

Atabay, O., Ötkür, M., and Ereke, M. İ. (2018). Model Based Predictive Engine Torque Control for Improved Drivability. *Proceedings of the Institution of Mechanical Engineers, Part D: Journal of Automobile Engineering*, *232*(12), 1654-1666.

Barbosa, S. R., & Machado, T. J. (2017). Limit Cycle Prediction of Systems with Fractional Controllers and Backlash. *Journal of Vibration and Control*, *23*(4), 587-603.

Batra, M., McPhee, J., & Azad, L. N. (2018). Real-time Model Predictive Control of Connected Electric Vehicles. *Vehicle System Dynamics*, *57*(10), 1720-1743.

Caruntu, F. C., Balau, E. A., Lazar, M., Bosch, P.j.v.d. P., & Cairano, D. S. (2016). Driveline Oscillations Damping: A Tractable Predictive Control Solution Based on a Piecewise Affine Model. *Nonlinear Analysis: Hybrid Systems*, *19*, 168-185.

Chamaillard, Y., Higelin, P., & Charlet, A. (2004), A simple method for robust control design, application on a non-linear and delayed system: engine torque control. *Control Engineering Practice, 12*(4), 417–429.

Chen, X., Peng, D., Hu, J., Li, C., Zheng, S., & Zhang, W. (2022). Adaptive Torsional Vibration Active Control for Hybrid Electric Powertrains during Start-up Based on

Model Prediction. *Proceedings of the Institution of Mechanical Engineers, Part D: Journal of Automobile Engineering*, *236*(10-11), 2219-2229.

Dhaouadi, R., Kudo, K., & Tobise, M. (1994). Analysis and Compensation of Speed Drive Systems with Torsional Loads. *IEEE Transactions on Industry Applications*, *30*(3), 760-766.

Formentini, A., Oliveri, A., Marchesoni, M., & Storace, M. (2017). A Switched Predictive Controller for an Electrical Powertrain System with Backlash. *IEEE Transactions on Power Electronics*, *32*(5), 4036-4047.

Gagliardi, G., Tedesco, F., & Casavola, A. (2022). H_∞ calibratable LPV control strategies for torque control in automotive turbocharged engines. *International Journal of Control, 95*(11), 3012-3029.

Hiramatsu, S., Nagamatsu, A., & Sumida, S. (2000). An Approach on Modeling for Functional Development of Automobile. *SAE Technical Paper*, *109*(6), 162-172.

Hirata, M., Hasegawa, T., & Nonami, K. (2005). Short Track-seeking Control of Hard Disk Drives by Using Final-state Control. *IEEJ Transactions on Industry Applications*, *125*(5), 524-529.

Hunang, X., Zhang, H., Zhang, G., & Wang, J. (2014). Robust Weighted Gain-Scheduling H_∞ Vehicle Lateral Motion Control with Considerations of Steering System Backlash-Type Hysteresis. *IEEE Transactions on Control Systems Technology*, *22*(5), 1740-1753.

Jung, M., & Glover, K. (2005). Calibratable Linear Parameter-Varying Control of a Turbocharged Diesel Engine. *IEEE transactions on control systems technology, 14*(1), 45-62.

Kaminer, I., Khargonekar, P. P., & Rotea, A. M. (1993). Mixed $H_2H\infty$ Control for Discrete-time Systems via Convex Optimization. *Automatica*, *29*(1), 57-70.

Kawamura,H., Ito, K., Karikomi, T., & Kume, T. (2011). Highly-responsive Acceleration Control for the Nissan Leaf Electric Vehicle. *SAE Technical Paper*, *2011-01-0397*. (doi: https://doi.org/10.4271/2011-01-0397)

Lagerber, A., & Egardt, B. (2007). Backlash Estimation with Application to Automotive Powertrains. *IEEE Transactions on Control Systems Technology*, *15*(3), 483-493.

Li, Y., Hansen, A., Hedrick, K. J., & Zhang, J. (2017). A Receding Horizon Sliding Control Approach for Electric Powertrains with Backlash and Flexible Half-shafts. *Vehicle System Dynamics*, *55*(12), 1823-1841.

Marini, F., & Walczak, B. (2015). Particle Swarm Optimization (PSO): A Tutorial. *Chemometrics and Intelligent Laboratory Systems*, *149*(B), 153-165.

Nishidome, C., & Kajiwara, I. (2003). Motion and Vibration Control of Flexible-Link Mechanism with Smart Structure. *JSME International Journal Series C Mechanical Systems, Machine Elements and Manufacturing*, *46*(2), 565-571.

Pan, T., Zang, H., Qiang, P., & Wu, P. (2022). Dual-objective Torque Control of Electric Vehicles Drivetrain with Robust Global Finite-time Stability Guarantee. *Vehicle System Dynamics*, *0*, 1-24.

Pham, T., Seifried, R., Hock, A., & Scholz. C. (2016). Nonlinear Flatness-Based Control of Driveline Oscillations for a Powertrain with Backlash Traversing. *IFAC-PapersOnLine*, *49*(11), 749-755.

Ponce, U. I., Orlov, Y., Aguilar, T. L., & Álvarez, J. (2016). Nonsmooth H_∞ Synthesis of Non-minimum-phase Servosystems with Backlash. *Control Engineering Practice*, *46*, 77-84.

Rodríguez, M. J., Meneses, R., and Orús, J. (2014). Active Vibration Control for Electric Vehicle Drivetrains. *IECON 2013 - 39th Annual Conference of the IEEE Industrial Electronics Society*, 2590-2595.

Rostalski, P., Besselmann, T., Barić, M., Belzen, V. F., & Morari, M. (2007). A Hybrid Approach to Modelling, Control and State Estimation of Mechanical Systems with Backlash. *International Journal of Control*, *80*(11), 1729-1740.

Seidl, R. D., Lam, L. S., Putman, A. J., & Lorenz. R. D. (1995). Neural Network Compensation of Gear Backlash Hysteresis in Position-Controlled Mechanisms. *IEEE Transactions on Industry Applications*, *31*(6), 1475-1483.

Shi, Y., & Eberhart, R. (1998). A Modified Particle Swarm Optimizer. *1998 IEEE International Conference on Evolutionary Computation Proceedings. IEEE World Congress on Computational Intelligence*, *No.98TH8360*, 69-73.

Shi, Y., & Eberhart, C. R. (1999). Empirical Study of Particle Swarm Optimization. *Proceedings of the 1999 Congress on Evolutionary Computation-CEC99*, *No.99TH8406*(3), 1945-1950.

Sumida, S., & Nagamatsu, M. (2001). A Modeling Approach on Modeling for Nonlinear System for Functional Development of Automobile. *SAE Technical Paper*, *2001-01-0638*. (doi: https://doi.org/10.4271/2001-01-0638)

Sumida, S., Hiramatsu, S., & Nagamatsu, M. (2002). Modeling for Functional Expression of Rotary Apparatus. *SAE Technical Paper*, *111*(6), 1243-1252.

Totani, T., & Nishimura, H. (1994). Final-State Control Using Compensation Input. *Transactions of the Society of Instrument and Control Engineers*, *30*(3), 253-260.

Trecate, F. G., & Gati, M. (2005). Observability Analysis and State Observers for Automotive Powertrains with Backlash: a hybrid system approach. *International Journal of Control*, *79*(5), 496-507.

Vadamalu, S. R., & Beidl, C. (2016). MPC for Active Torsional Vibration Reduction of Hybrid Electric Powertrains. *IFAC-Papers Online*, *49*(11), 756-761.

Vansevich, V. V. (2014). Vehicle Systems: Coupled and Interactive Dynamics Analysis. *Vehicle System Dynamics*, *52*, 1489-1516.

Vörös, J. (2010). Identification of cascade systems with backlash. *International Journal of Control*, *83*(6), 1117-1124.

Wang, J., Duan, Z., Zhao, Y., Qin, G., & Yan, Y. (2013). H_∞ and H_2 control of multi-agent systems with transient performance improvement. *International Journal of Control*, *86*(12), 2131-2145.

Wu, S. T., Karkoub, M., Wang, H., Chen, S. H., & Chen, H. T. (2017). Robust Tracking Control of MIMO Underactuated Nonlinear Systems with Dead-Zone Band and Delayed Uncertainty Using an Adaptive Fuzzy Control. *IEEE Transactions on Fuzzy Systems*, *25*(4), 905-918.

Yamaguchi, A., Ohishi, K., Yokokura, Y., & Miyazaki, T. (2019). Backlash-based Shock Isolation Control for Jerk Reduction in Clutch Engagement. *IEEJ Journal of Industry Applications*, *8*(2), 160-169.

Yonezawa, H., Kajiwara, I., Sato, S., Nishidome, C., Sakata, M., Hatano, T., & Hiramatsu, S. (2019). Vibration Control of Automotive Drive System with Nonlinear Gear Backlash. *Journal of Dynamic Systems, Measurement, and Control*, *141*(12), 121002-121012.

Zietkiewicz, J., Kozierski, P., & Giernacki, W. (2020). Particle Swarm Optimization in Nonlinear Model Predictive Control: Comprehensive Simulation Study for Two Selected Problems. *International Journal of Control*, *94*(10), 2623-2639.

Zuppa, A. L., Ikhouane, F., & Pujo, G. (2013). Robust Control Design for Mechanisms with Backlash. *Journal of Control Engineering and Technology*, *3*(4), 175-180.